Analysis of stimulated Raman scattering using diode data at the Pecos experimental platform

D. E. Davis, ¹ J. R. Fein, ² D. E. Ruiz, ² M. Geissel, ² A. J. Harvey-Thompson, ² and K. Peterson ²

¹University of New Mexico, School of Engineering, Albuquerque, New Mexico 87106, USA

²Sandia National Laboratories, Albuquerque, New Mexico 87123, USA

(Dated: September 17, 2018)

In order to increase neutron yield in fusion experiments on the Magnetized Linear Inertial Fusion (MagLIF) platform, it is important to maximize the energy coupled to the fuel during the laser-preheat stage. However, laser-energy coupling is limited by laser—plasma instabilities (LPI). In this regard, the Pecos facility at Sandia National Laboratories uses the Z-beamlet laser to test and study the effects of LPI on MagLIF-relevant targets. In particular, stimulated Raman scattering (SRS) is measured in Pecos by using two photo-diodes and a near-beam imager. The measurements from the photo-diodes are processed using a synthetic spectrum based on a Gaussian model. With this relatively simple model, the mean wavelength and intensity of backscattered light can be deduced. Our measurements show similar trends as those given by time-resolved spectrometer data. Hence, this model provides a simple way to approximate time-resolved spectra for scattered light by SRS.

I. INTRODUCTION

In fusion experiments on the Magnetized Liner Inertial Fusion (MagLIF) platform, a cylinder of deuterium gas with a pre-imposed 10 T axial magnetic field is heated using a 2.5 kJ, 1 TW laser, and magnetically imploded by a 19 MA, 100 ns rise time current on the Z facility [1, 2]. In order to achieve higher neutron yields in MagLIF, it is important to maximize the energy delivered from the Z-beamlet laser to the fuel. However, laser—plasma interactions (LPI) are known to cause a detrimental effect on laser-energy deposition [3]. A signature of LPI and decreased energy deposition is the amount of light backscattered due to stimulated Raman scattering (SRS). Since part of the incident laser energy is scattered, this reduces the efficiency of energy deposition to the MagLIF fuel [3]. Having a quantitive measure of SRS can give better insight into the plasma conditions and the laser-energy deposition.

In the Pecos facility at Sandia National Laboratories, offline experiments are done in order to study the effects of LPI on MagLIF-relevant targets [3]. Although the Pecos facility has implemented two photodiodes to measure stimulated Raman backscatter, the data had not yet been fully analyzed. In this work, the time-resolved measurements from the two photo-diodes were processed using a synthetic spectrum based on a Gaussian model. From this relatively simple model, we were able to deduce the mean wavelength and intensity of the scattered light. Our measurements show similar trends to data obtained using the time-resolved SRS spectrometer. From this method, trends seen in synthetic SRS spectra characteristics can give better insight on LPI.

There is still much to be learned from the Pecos diode data that could give further insight into LPI. In future analysis, the NBI data could be incorporated into the Gaussian model in order to refine our model. This method can also be used for studying SBS light emission, as well as X-ray emissions in experiments conducted in

Pecos.

The present paper is organized in the following manner. In Sec. II, the basic theory of SRS will be introduced. In Sec. III, an introduction to the Pecos experimental setup is given. Sec. IV provides details on the methods used to perform the data analysis. In Sec. V, the results of the analysis are discussed. A conclusion for this work is given in Sec. VI.

II. BASIC THEORY

In the following, I shall provide a basic overview of the SRS instability. SRS is produced by the nonlinear coupling of two electromagnetic waves with an electron Langmuir wave in a plasma. The frequency and wavevector matching conditions of SRS are determined by the following:

$$\omega(\mathbf{k_0}) = \omega_{\rm EM}(\mathbf{k_s}) + \omega_{\rm L}(\mathbf{k}), \tag{1}$$

$$\mathbf{k_0} = \mathbf{k_s} + \mathbf{k}.\tag{2}$$

Here $\mathbf{k_0}$, $\mathbf{k_s}$ and \mathbf{k} are the wavevectors of the incident light, the scattered light, and the Langmuir wave, respectively. The dispersion relation for the EM wave is

$$\omega_{\rm EM}^2(\mathbf{k}) = c^2 k^2 + \omega_{\rm pe}^2,\tag{3}$$

where $k \doteq |\mathbf{k}|$ and

$$\omega_{pe} \doteq \sqrt{\frac{4\pi e^2 n_0}{m_e}},\tag{4}$$

is the electron plasma frequency. The electron mass and charge are represented by m_e and e, respectively. The background density is denoted by n. Similarly, the dispersion relation for Langmuir waves is

$$\omega_{\mathcal{L}}^2(\mathbf{k}) = 3v_{\mathcal{T}}^2 k^2 + \omega_{\mathcal{p}e}^2,\tag{5}$$

where $v_{\rm T}$ is the thermal velocity. Using the approach in Ref. [4], when Eqs. 1 and 2 are satisfied, then the growth rate of the scattered light due to the SRS growth is given by

$$\gamma = \frac{k v_{os}}{4} \sqrt{\frac{\omega_{\rm pe}^2}{\omega_{\rm L}(\omega - \omega_{\rm L})}},\tag{6}$$

where γ is the growth rate and $v_{\rm os}$ is the oscillatory velocity $v_{\rm os} = qA_0/m_{\rm e}$.

Using Eq. (1) and Eq. (4)

$$n_e = n_c \left(1 - \frac{\lambda_0}{\lambda_s} \right)^2 \tag{7}$$

is derived. Where n_e is the critical laser density, λ_0 is the wavelength of the incident laser, and λ_s is the wavelength of the scattered laser light.

III. PECOS EXPERIMENT PLATFORM

A. General overview of Pecos

The Pecos facility is used to study the laser pre-heating stage for MagLIF targets. The advantage of performing offline experiments on Pecos is that the facility allows for better access for diagnostics to study LPI and other laser—target interactions. As shown in Fig. 1, the Pecos chamber utilizes the 526.6 nm Z-beamlet (shown as ZBL) laser to deliver laser energy to the target. A secondary laser (the Chaco laser) is used as a back light for diagnostics, including shadowgraphs.

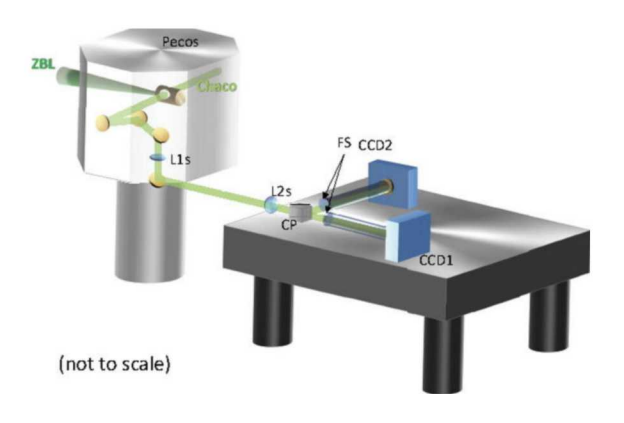


FIG. 1: General schematic of the Pecos facility.

B. SRS diodes

Two diodes are utilized to measure the laser light scattered due to SRS. The diodes are placed next to one another on the backside of the Pecos chamber facing the scatter plate (see Fig. 2). Both diodes utilize filters to sample a narrow wavelength band of approximately 600 to 700 nm (see Fig. 3). A thick Schott filter is also used to drastically reduce the SRS transmission.

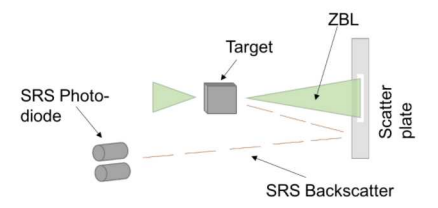


FIG. 2: Schematic of the location of the two SRS diodes.

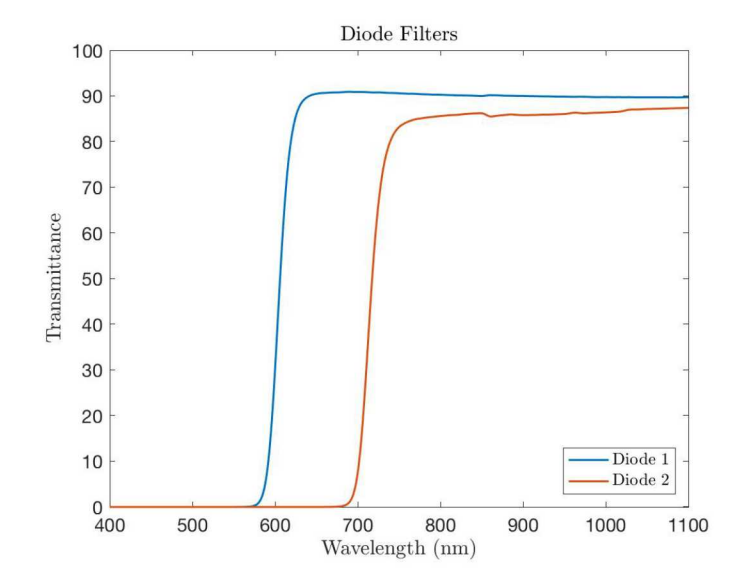


FIG. 3: Filter transmittance for each diode as a function of wavelength.

IV. DATA ANALYSIS

In order to interpret the voltage signals $v_i(t)$ measured by the SRS diodes, we model the measured signal of the *i*-th diode using the expression

$$V_i(t) = c \int K_i(\lambda) S(\lambda, t) d\lambda$$
 (8)

where $S(\lambda,t)$ is the time-dependent spectrum of the emitted SRS light and K_i is the quantum transmittance of the i-th diode. For our modeling purposes, the SRS spectrum is described using a simplified Gaussian model

$$S(\lambda, t) = A(t) e^{-(\lambda - \mu(t))^2 / \sigma(t)^2}, \tag{9}$$

where A(t) is the amplitude of the spectrum, $\mu(t)$ is the mean wavelength, and $\sigma(t)$ denotes the width of the spectrum. Also, the quantum transmittance is given by

$$K_i(\lambda) = T(\lambda) Q E_i(\lambda),$$
 (10)

where $T(\lambda)$ is the total transmittance of the Schott filter and the long-pass filter located in front of the diodes and Q_i is the quantum efficiency of the *i*-th diode. As shown in Eq. (8), the voltage measured by diodes is dependent on the parameters of the Gaussian model for the SRS spectrum.

At each time step, voltage data from each diode was used to solve for λ and μ while keeping σ constant. From previous spectrometer data, it was found that an approximate mean value $\sigma=10nm$ for all time was appropriate. Of course, σ is expect to change in time. However, not enough information was currently present to also solve for σ . The mean wavelength λ and amplitude μ were solved by minimizing the following:

$$\chi(t)^{2} = \sum_{n=i} |\frac{v_{i}(t) - V_{i}(t)}{\sigma_{i}^{2}}|^{2}.$$
 (11)

In order to validate the model, I constructed a synthetic voltage signal created with a curve with known parameters. Then, the algorithm described was used to recreate the amplitude and wavelength of the synthetic signal. This test was successful.

A. Voltage Signal Processing

In order to smooth the signal from the SRS diodes, a Gaussian was fit to the raw voltage responses. Although this is not a physical representation of a diode response, fitting a Gaussian to the data allowed for better model response and resolution. The fitted Gaussian curves can be seen in the two red curves in Fig. 4. Both the smoothed data and the raw data were processed using the algorithm described above. A more in-depth analysis of the results will be discussed in Sec. V.

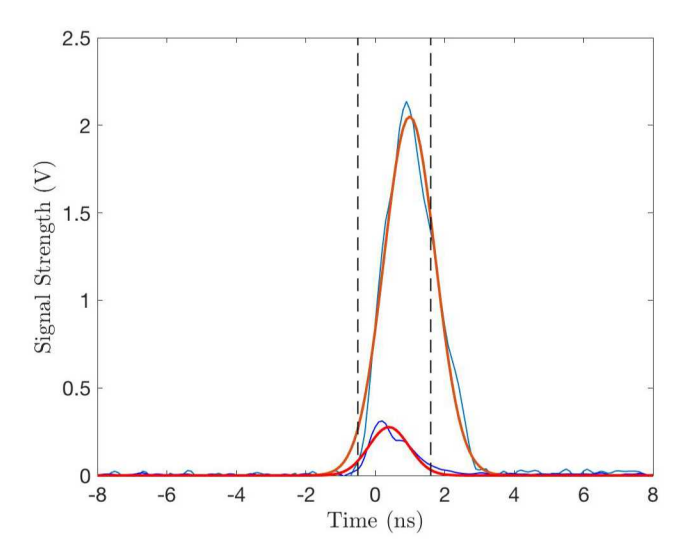


FIG. 4: An image of both diode voltage traces and the corresponding confidence window. The red curves depict the Gaussian fit data. The blue curves depict the raw data.

A confidence window was added to the diode trace to create a trust region for the model to operate within. The window is based on a minimum threshold dictated by the peak diode voltage of the weaker signal and noise level. Data to the sides of the wings are taken to be within the noise threshold of the voltage signal. This window can be seen in the dashed, black lines in Fig. 4.

B. Model Parameters

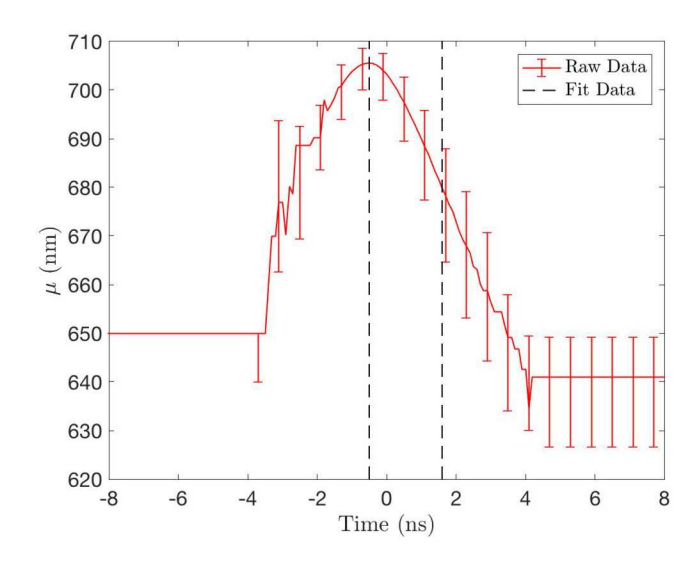


FIG. 5: Mean wavelength $\mu(t)$ as a function of time.

In the following, we shall apply the model data–processing model to the SRS diode measurements for Pecos shot B18050803. In Fig. 5 an, almost linear downward trend can be seen in μ inside the confidence window. The lower error bar is relatively low at the start of the confidence window and increases in time. This figure was created using the Gaussian voltage signal. The error bars were created with an upper bound of $\sigma = 5nm$ and lower bound of $\sigma = 10nm$ centered at $\sigma = 10nm$.

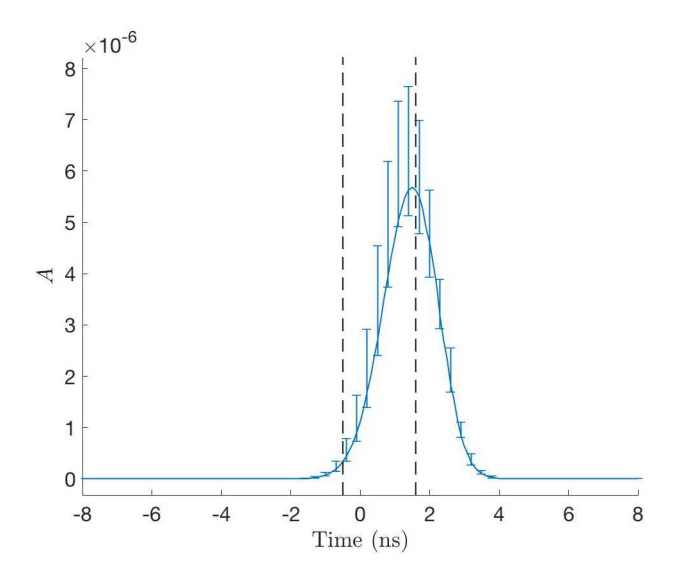


FIG. 6: Intensity A(t) as function of time.

The opposite trend can be seen in the intensity of the spectra in Fig. 6, using the Gaussian voltage signal. The intensity begins relatively low and grows exponentially to the peak value within the confidence window. Also, take note that the upper error bars increase in time.

C. Model Convergence

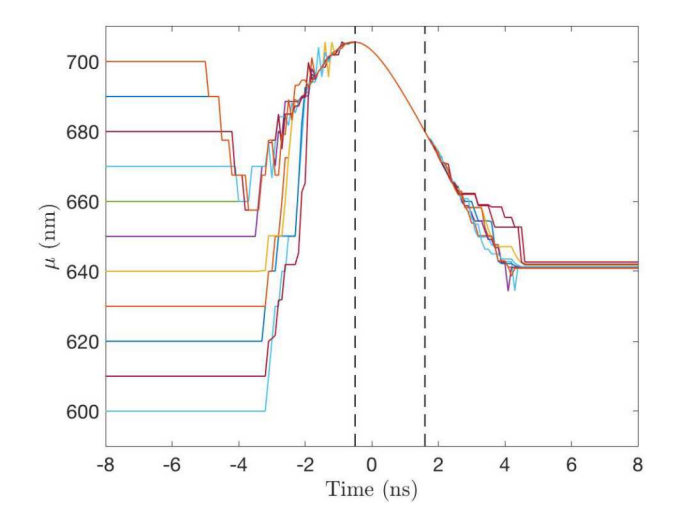


FIG. 7: Varying the initial guess for μ does not lead to different results within the confidence window.

One could argue that there could be a possibility that the minimization of χ^2 in Eq. (11) does not lead to a unique solution. To show this is not the case, I varied the initial guess for μ . As seen in Fig. 7, the solution within the trust window does not vary. Hence, it appears μ converges to an exact solution in the trust window.

D. Model Trends

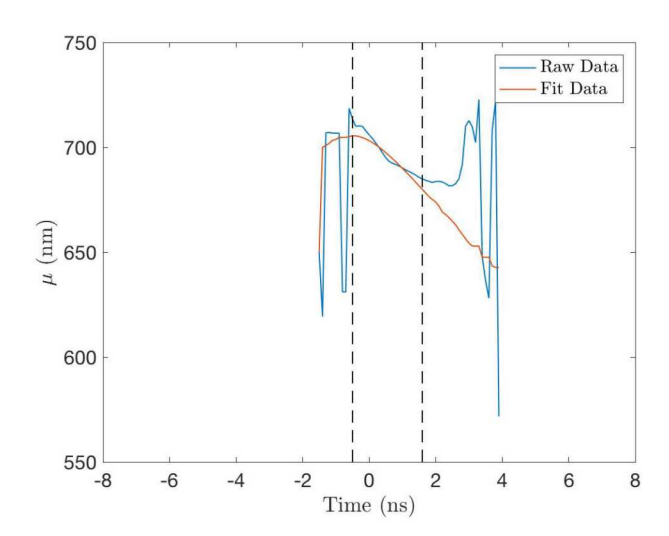


FIG. 8: Obtained mean wavelength $(\mu(t))$ using the raw diode data and the fit diode data.

In Fig. 8, one can see μ generated using the raw diode data and the Gaussian fit to the diode data. Both the raw and fit data follow similar trends within the error window (see Fig. 5). Outside the error window the smoothed data follows a continuous trend. However, the raw data appears to be disrupted by the acquisition noise. These trends were observed across several Pecos shots using different laser energy, laser entrance hole (LEH) thickness, pulse length, and gas type and density.

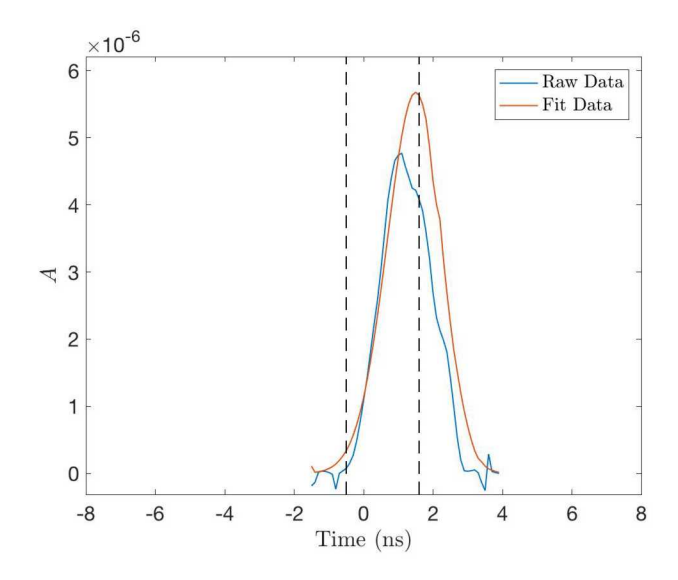


FIG. 9: Obtained amplitude (A(t)) using the raw diode data and the fit diode data.

As seen in Fig. 9, similar trends are observed in shape between the raw and fit intensity. However, one should not that the fitted data gives higher peak intensities.

These trends were also observed across all analyzed Pecos shots.

In Figs. 10 and 11, I show the time evolution of the spectra parameters for multiple shots. The following plots compare spectra parameter trends for multiple shots. In Fig. 10, wavelength is converted to density using Eq. (7).

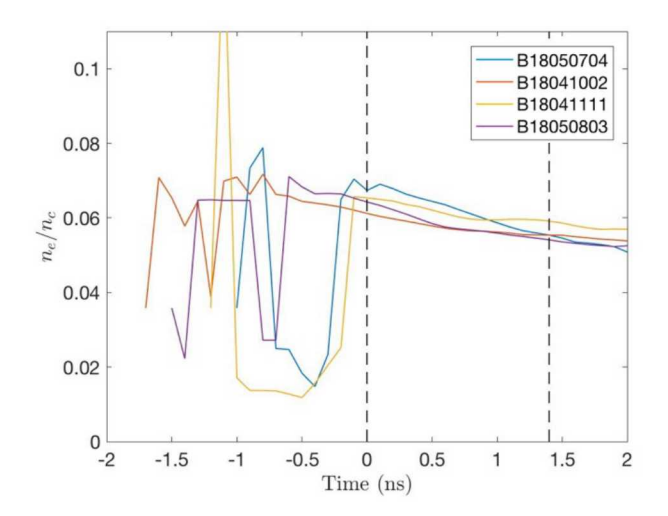


FIG. 10: Comparison of density (n_e/n_c) for four different analyzed shots.

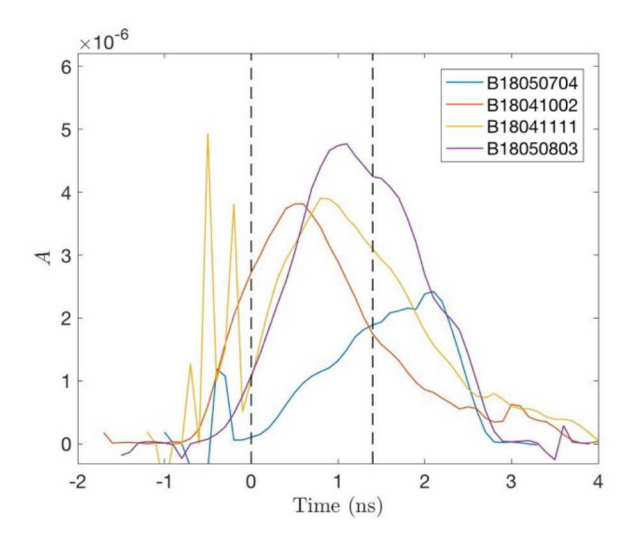


FIG. 11: This is a comparison of changes in intensity (A) for four different analyzed shots.

V. DISCUSSION

A. Micro-physics of LPI

Using the signal from the diode traces, this analysis produced synthetic Gaussian spectra for SRS. Trends in both μ and A can hint toward plasma conditions. In

Fig. 5, one can see that the wavelength decreased in an almost linear fashion. From Eqn. Eq. (7), it can be inferred that the plasma electron density also decreased within the time window. Because the data is not spatially resolved, we do not know the origin of the SRS signal. However, a decrease in plasma density is consistent with the theoretical physics of LPI. We expect to see a decrease in plasma density due to thermal expansion. However, it is also possible that the SRS signal is the consequence of laser filamentation. In which case, we would also expect a decrease in plasma density.

In previously analyzed spectrograph data, we see similar trends in mean wavelength and intensity. The mean wavelength decreases in the spectrograph data, similar to the model parameter μ (see Fig. 8). It is also seen that the intensity of the SRS spectra ramps to a peak value, where the SRS signal is saturated, and then begins to decrease again in time. This behavior is seen in the intensity of the spectra in the model parameter A.

In Figs. 10 and 11, the trend in mean wavelength (μ) and intensity (A) is compared in multiple shots. The shots where chosen to vary in laser energy. Also, all shots use a 1.1 mm distributed-phase plate (DPP) except B18050803, which uses a .75 mm DPP. One can see that the density decreases from 7.6 percent critical density to 6 percent critical density on a time scale of roughly 2 ns across all shots. The model predicts a similar decrease in plasma density for shots with varying laser energy. This trend is also apparent in some spectrograph data. However, a direct comparison for spectrograph data and SRS diode data of the same shot does not vet exist. The intensities A of the analyzed shots in Fig. 11 share a similar shape; the intensity increases until saturation and then decreases to zero. Shot B18050803 and shot B18050704 share similar laser energies. However, the sixty six percent increase in intensity can be explained by the difference in DPP diameter. The lower diameter phase plate may cause more filamentation within the plasma giving rise to a higher SRS signal.

Comparing the model results to time-resolved spectrograph data can give further verification of trends seen in mean wavelength and SRS intensity. The comparison can also prove the physicality of what is seen in the synthetic spectra.

B. Analysis of shot trends in Pecos

A shot-to-shot analysis of SRS photo-diode was conducted comparing laser energy and initial gas-fill pressure of deuterium. As shown in Figs. 12 and 13, an increase in laser energy corresponds to an increase in peak voltage of the SRS diode trace. We see more SRS signal with higher laser energy. Similarly, we see a direct correlation between the integrated voltage of the smoothed SRS voltage trace and laser energy. The trend line for integrated voltage follows the same shape as the trend line for laser energy, but has a shallower rise. This may be

explained by an increase in peak voltage but a relatively constant width of the diode voltage trace.

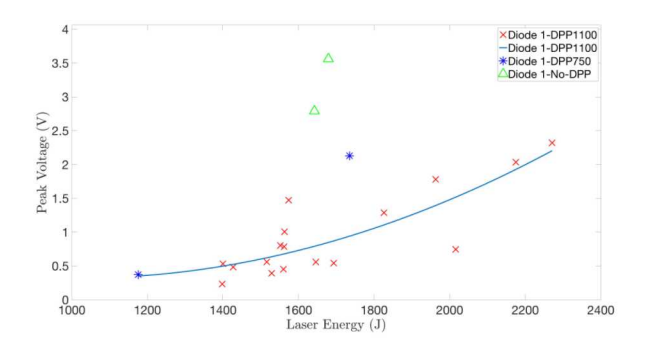


FIG. 12: The comparison of shot-to-shot trends of laser energy and peak voltage.

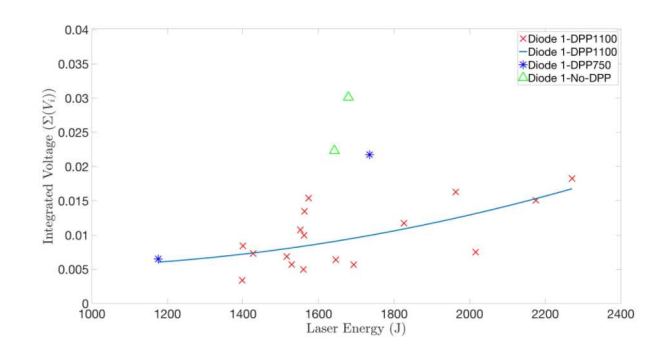


FIG. 13: The comparison of shot-to-shot trends of laser energy and integrated voltage.

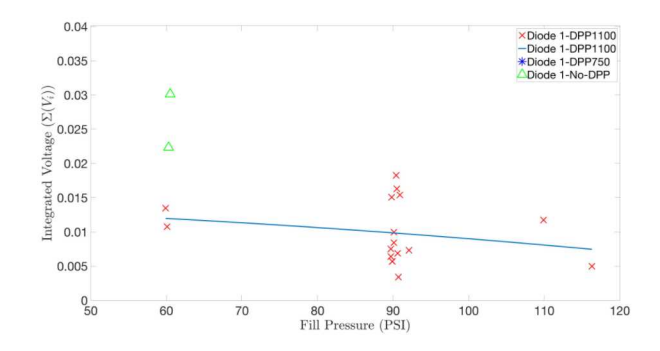


FIG. 14: This is a plot comparing the shot-to-shot trends in the initial fill pressure and the integrated diode trace.

In Fig. 14, a possible trend in integrated voltage may be seen. However, since all data points are centered around three fill pressures, we do not have enough information to confirm this trend. Also, this data is not separated by LEH window thickness, pulse length or coinjection. But it is important to note that the shots that do not incorporate a DPP have a higher SRS signal seen in the peak voltage and integrated voltage for laser energy and initial fill pressure.

VI. CONCLUSIONS

Two photo-diodes were used to ascertain synthetic SRS spectra by utilizing the two different transmission curves produced by long pass filters. The synthetic SRS spectrum was approximated using a simple Gaussian. The parameters for the Gaussian were solved for by minimizing the square difference in voltage created by the synthetic SRS spectra and the SRS diode voltage. From the model, it was observed that the mean wavelength μ decreased in time within a confidence window. This decrease in mean wavelength follows the theory behind plasma conditions, where the density is expected to decrease in time due to thermal expansion. It was also observed that intensity A increased until the SRS saturation point and then decreased back to zero. These trends were also observed in spectrograph data.

There is still much to be desired from this model in terms of verification and better characterization of the synthetic spectra. However, this model gives a baseline for parameters in the SRS spectra that can tell us useful information about laser—plasma coupling and plasma conditions. Future applications of this work may include more data points from the NBI and other Pecos diagnostics to better characterize the synthetic spectra. It may also be interesting to see this analysis method applied to SBS and X-Ray diode data.

Acknowledgments

This work was supported by the U.S. DOE through Contract DE-AC02-09CH11466 and by Sandia National Laboratories. Sandia National Laboratories is a multimission laboratory managed and operated by National Technology and Engineering Solutions of Sandia, LLC., a wholly owned subsidiary of Honeywell International, Inc., for the U.S. DOE National Nuclear Security Administration under contract DE-NA-0003525. This paper describes objective technical results and analysis. Any subjective views or opinions that might be expressed in the paper do not necessarily represent the views of the U.S. Department of Energy or the United States Government.

- S. A. Slutz, M. C. Herrmann, R. A. Vesey, A. B. Sefkow, D. B. Sinars, D. C. Rovang, K. J. Peterson, and M. E. Cuneo, "Pulsed-power-driven cylindrical liner implosions of laser preheated fuel magnetized with an axial field," Phys. Plasmas 17, 056303 (2010).
- [2] M. R. Gomez, S. A. Slutz, A. B. Sefkow, D. B. Sinars, K. D. Hahn, S. B. Hansen, E. C. Harding, P. F. Knapp, P. F. Schmit, C. A. Jennings, et al., "Experimental demonstration of fusion-relevant conditions in magnetized liner
- inertial fusion," Phys. Rev. Lett. 113, 155003 (2014).
- [3] M. Geissel, A. J. Harvey-Thompson, T. J. Awe, D. E. Bliss, M. E. Glinsky, M. R. Gomez, E. Harding, S. B. Hansen, C. Jennings, M. W. Kimmel, et al., "Minimizing scatter-losses during pre-heat for magneto-inertial fusion targets," Phys. Plasmas 25, 022706 (2018).
- [4] W. L. Kruer, *The Physics of Laser Plasma Interactions* (Addison-Wesley Publishing Co., 1988).